Characteristics and Catalytic Properties of Ni/$CaAlO_x$ Catalyst for Hydrogen-enriched Syngas Production from Pyrolysis-steam Reforming of Biomass Sawdust

Fangyuan Chen[a,d], Chunfei Wu[b*], Lisha Dong[a], Anthony Vassallo[a], Paul T. Williams[c*], Jun Huang[a*]

[a]School of Chemical and Bimolecular Engineering, University of Sydney, Australia, NSW 2037 (Tel: +61 2 9351 7483; Email: jun.huang@sydney.edu.au)

[b]School of Engineering, University of Hull, HU6 7RX,, UK (Tel: +44 1482 466464; Email: c.wu@hull.ac.uk)

[c]School of Chemical & Process Engineering, University of Leeds, Leeds LS2 9JT, UK (Tel: +44 113 3432504; Email: p.t.williams@leeds.ac.uk)

[d]School of Environmental Science & Engineering, Kunming university of Science & Technology, Kunming 650038, P. R. China

Abstract: The production of hydrogen-enriched syngas from the thermo-chemical conversion of biomass was studied using Ni/$CaAlO_x$ catalysts prepared by co-precipitation method. The effect of Ca addition with different molar ratios of Ca:Al (1:3, 1:2, 1:1, 2:1, 3:1) on the properties and catalytic behaviour in relation to syngas production and the coke formation on the surface of the catalysts were investigated. Catalysts were characterized by BET, XRD, TPR, SEM, and TEM. The SEM and TEM results showed that rod-shaped nano-particles were highly dispersed on the surface of the catalyst. The particle size of NiO was slightly affected with the increase of Ca content in the catalyst. It appeared that the selectivity of CO was increased and the selectivity of CO_2 was reduced with the increase of Ca addition to the catalyst. For example, CO_2 concentration was reduced from 20 to 12 Vol.%, when the molar ratio of Ca/Al was increased from 1:3 to 3:1 for the Ni/$CaAlO_x$ catalyst; it is suggested that the water gas shift reaction was inhibited and CO_2 reforming reactions were promoted in the presence of the catalyst with higher Ca content. The CO/H_2 molar ratio could be manipulated by changing the Ca content in the catalyst, while the H_2 concentration remained almost constant (around 45 Vol.%). Thus, using the Ni/$CaAlO_x$ catalyst developed in this work could provide a promising route to control the syngas composition, which is an important factor for syngas applications.

Keywords: Biomass; Pyrolysis; Co-precipitation; Calcium: Ni-catalyst

1. Introduction

The consumption of fuels and chemicals continues to increase with the development of the world's economy [1, 2]. As a versatile building block in the chemical industry and fuel synthesis, synthesis gas (syngas) plays an important role in industry [3-5]. Currently, syngas production largely depends on fossil sources through the reforming process [6]. For sustainable development, great attention has been focussed on the production of syngas from renewable resource. Biomass, including agriculture and forest wastes is one of the most abundant renewable resources; it has been considered as a promising raw material to partially replace fossil resources in syngas production in the future [7-12].

Biomass gasification has been widely practiced for syngas production due to its high thermal efficiency [12]. However, this process has challenges towards large-scale development, i.e. low hydrogen production and high tar content in the syngas [13, 14]. Catalysts are well-known for their capability for accelerating biomass conversion through lowering activation energy, and for enhancing catalytic reforming to produce syngas [12, 15, 16]. For example, reduction of tar and significant increase in production of syngas have been achieved by adding olivine and alumina catalysts to biomass gasification using a conical spouted bed reactor [15]. Cheah et al. [17] carried out biomass gasification using a nickel cerium olivine catalyst; they reported that the presence of catalyst resulted in a significant improvement of H_2-enriched syngas production. In addition, the improvement of hydrogen production was reported by adding Fe/CaO catalyst to a continuous-feed fluidized bed reactor [16]. Supported noble metal catalysts such as Rh, Ru and Pt have been reported to effectively increase syngas yield [18-21]. However, the high cost of these noble metals limits the wide applications of biomass gasification in industrial practice.

At present, low-cost transition metal catalysts such as Ni-based catalysts have been widely used as effective alternatives to noble metal-based catalysts in biomass gasification or steam reforming processes [14, 22]. Ni based catalysts are generally prepared by impregnation method by loading Ni or NiO particles on catalyst supports such as alumina and silica for gasification or reforming. The physical structure and

chemical composition of catalyst supports influence the characteristics of Ni catalysts e.g. Ni dispersion and consequently their catalytic performance for gas production from biomass gasification. For a better Ni dispersion, various nano-porous supports such as MCM-41 [23, 24], zeolite [25], and SBA-15 [26, 27] have been utilized to confine the size of Ni nano-particles inside the pores of the catalyst support. This type of confined reaction space with uniform Ni particles could enhance the production of H_2-enriched syngas. However, the nanopores of catalysts have diffusion limitations for large-molecular weight biomass compounds and thus reduce the catalytic performance for syngas production [13].

Another efficient method to enhance Ni dispersion is to induce a strong metal-support interaction by incorporating rare-earth or alkaline metals in the catalyst system. It has been reported that introducing Zr, Ce, and Mg into a silica support markedly promoted Ni dispersion [28-31]. Based on these previous contributions, it is desirable to prepare a highly dispersed Ni catalyst using non-porous supports without diffusion limitation. However, using rare-earth metals as promoters to Ni-based catalysts is costly. In this study, we introduced Ca, a low cost and highly abundant metal, into alumina supports for preparing uniform and fine Ni nano-particles with high dispersion for H_2-enriched syngas production from biomass through a pyrolysis-reforming process, using a two-stage reaction system.

2. Experimental

2.1 Biomass sample and catalyst synthesis

Wood sawdust with a size less than 0.2 mm was used as raw biomass material in this work. The biomass sample contained 6.4 wt.% moisture, 74.8 wt.% volatiles, 18.3 wt.% fixed carbon and 1.2 wt.% of ash, as reported in our previous work [24]. In addition, the biomass contents of C, H, O and N were 47.1, 5.9, 46.9 and 0.1 wt.%, respectively.

The catalysts were prepared by a co-precipitation method with an initial Ni-loading mole ratio of 20 mol%. Ni $(NO_3)_3 \cdot 6H_2O$(≥99%), Ca $(NO_3)_3 \cdot 4H_2O$(≥99%),

$Al_2(NO_3)_3 \cdot 9H_2O$(≥99%) were purchased from Sigma-Aldrich. Precursors with the desired Ni-Ca-Al ratios were prepared by dissolving a certain amount of metal salts in deionized water. After the precipitation, the suspension was aged under agitation for an hour and then filtered under vacuum. The filter cake obtained was rinsed with deionized water several times followed by drying at a temperature of 80 °C overnight. The solid products were calcined at 800 °C for 4h with a heating rate of 1 min^{-1} in static air. The catalysts obtained were labeled as Ni/$CaAlO_x$(A:B), where A:B represented the mole ratio of Ca to Al.

2.2 Catalyst characterization

BET surface area of the fresh catalysts was analyzed by N_2 adsorption and desorption isotherms on a Quanta chrome Autosorb-1. X-Ray Diffraction (XRD) analysis was carried out by using a SIEMENS D5000 in the range of 10°-70° with a scanning step of 0.02° using Cu Kα radiation (0.1542 nm wavelength). A scanning electron microscope (SEM) (LEO 1530) coupled to an Energy Dispersive X-ray spectroscope (EDXs) system was used to investigate the surface morphology and the element distributions of the catalysts. Temperature programmed reduction (TPR) using H_2 was employed to analyze the reduction behavior of the fresh catalysts by using a modified thermogravimetric analyzer (SDT Q600); during the TPR experiment, fresh catalysts were loaded in an alumina pan and placed in the thermogravimetric analyzer furnace which was purged by a gas flow containing 15% H_2 and 85% N_2 with a flow rate of 100 mL min^{-1}, and heated from room temperature to 900 ^oC at a heating rate of 10 ^oC min^{-1}.

Temperature-programmed oxidation (TPO) of the reacted catalysts was carried out using a Stanton-Redcroft thermogravimetric analyzer (TGA and DTG) to determine the properties of the reacted catalysts. About 10 mg of the reacted catalyst was heated in an atmosphere of air at 15 °C min^{-1} to a final temperature of 800 °C, with a dwell time of 10 min.

2.3 Experimental process

Pyrolysis-reforming of biomass was carried out with a fixed bed, two-stage reaction system. The first stage involved pyrolysis of the biomass and the pyrolysis gases were passed directly to the second stage where catalytic reforming took place as reported in our previous work [32]. During the experiment, N_2 (80 ml min^{-1}) was used as carrier gas. 0.5 g of biomass was placed inside a crucible and held in the first pyrolysis reactor. 0.25 g of sand or catalyst was placed in the second reactor. The temperature of the second reactor was initially heated to the set point (800 °C). Then the first reactor was heated to the pyrolysis temperature (500 °C) at a heating rate of 40 °C min^{-1} and kept at that temperature for 30 min. Water for steam reforming was injected into a location between the two reactors with an injection rate of 0.05 g min^{-1} when the temperature of the pyrolysis reactor reached 150 °C.

The products from pyrolysis/catalytic reforming were cooled using air and dry ice to collect the condensed liquid. Non-condensed gases were collected using a Tedlar^{TM} gas sample bag. Around 20 min more time was allowed to collect the non-condensed gases to ensure complete reaction. The amounts of injected water and the condensed liquid were calculated by weighing the syringe and condensers before and after the experiment, respectively. Experiments were repeated to ensure the reliability of the results.

Non-condensed gases collected in the Tedlar^{TM} gas sample bag were analysed off-line by gas chromatography (GC). H_2, CO and N_2 were analyzed with a Varian 3380 GC on a 60-80 mesh molecular sieve column with argon carrier gas, whilst CO_2 was analyzed by another Varian 3380 GC on a HayeSep 80-100 mesh column with argon carrier gas. C_1-C_4 hydrocarbons were analyzed using a Varian 3380 gas chromatograph with a flame ionization detector, with an 80-100 mesh HyeSep column with nitrogen carrier gas.

3. Results and discussion

3.1 Textural properties of Ni/CaAlO$_x$ catalysts

The BET surface areas of the Ni/$CaAlO_x$ catalysts were between 46 and 83 $m^2 g^{-1}$ and are reported in Table 1. It seems that the BET surface area did not change proportionally with the increase of Ca content in the catalyst support.

XRD patterns of the Ni/$CaAlO_x$ catalysts shown in Figure 1 may be used to identify the crystal species present in the catalysts. It can be seen that the main phases on the catalysts were CaO, $Ca(OH)_2$, NiO, and $NiAl_2O_4$NiO was present as separated metal particles and there were no detectable alloyed or inter-metallic Ca-Ni nanoparticles present. It should be noted that the catalysts were not pre-reduced prior to the experiments, and the NiO particles will be converted into active Ni particles by the produced H_2 and CO during the process of pyrolysis-reforming of biomass [33]. The diffraction peaks at 2 theta values of 32.2°, 53.9°, 64.2° and 67.5° were identified as CaO, and the diffraction peaks at 2 theta positions of 18.1°, 28.7°, 34.2°, 47.2° and 50.9° were identified as $Ca(OH)_2$. $Ca(OH)_2$ present on the catalysts may be derived from the hydrolysis of CaO by ambient moisture in the environment [34]. It was noted that $CaCO_3$ was not observed from XRD analysis of all the fresh catalysts. It has been reported that carbonation of CaO is slower compared with rapid hydration and the generated $Ca(OH)_2$ layer may act as a protective layer to prevent carbonation of CaO [34]. The diffraction peaks at 2 theta values of 37.3°, 43.3°, and 62.9° are assigned to NiO. The broad characteristics of the NiO peaks demonstrated a low crystallinity and high distribution of metal phases. In addition, the diffraction peaks at 2 theta values of 37.0°, 45.0°, 59.6° and 65.5 ° were assigned to $NiAl_2O_4$.

With the increase of Ca content changing from the Ni/$CaAlO_x$ (1:3) to Ni/$CaAlO_x$ (3:1), the peak intensity of CaO and $Ca(OH)_2$ increased. In contrast, the peak intensity and position of NiO barely changed when the Ca/Al ratio was increased from 1:3 to 3:1, indicating that there were only slight differences of size and distribution of NiO for the catalysts with different Ca contents. This corresponds with the calculated sizes of NiO particles (around 10 nm) from XRD analysis (Table 1). However, it was reported that the size of NiO can range widely over many nanometers depending on the composition of the catalysts [35, 36]. Wu et al. [37] have reported that when using Ni/La_2O_3 prepared by impregnation methods for glycerol steam reforming, the partial substitution of La by Ca

caused gradual increase of Ni particle size and significantly affected catalyst metal dispersion. Kariny et al. [38] reported that Ni-Ca/Al_2O_3 catalyst prepared by impregnation method has an increased size of Ni with the increasing of Ca content. It is demonstrated that the addition of Ca in the Ni/$CaAlO_x$ prepared by co-precipitation method in this work may favour size uniformity and dispersion of Ni, which are beneficial for catalytic reactions for syngas production from thermo-chemical conversion of biomass, as more active catalytic sites are available. High metal dispersion in the Ca-added catalysts prepared by co-precipitation makes Ca a promising candidate as a catalyst promoter. In addition, maintaining the size of active sites in the Ni/$CaAlO_x$ catalyst enables a controlled investigation into the influence of different amounts of Ca addition to the catalyst in relation to syngas production with little interference from the particle size of the active metal sites.

Figure 2 shows SEM images of the fresh Ni/$CaAlO_x$ catalysts. The surfaces of the catalysts were covered with fine spherical particles. The size of the spheres was around 100 nm. Limmanee et al.[34] has reported that substitution of Mg^{2+} and Zn^{2+} with Ca^{2+} resulted in highly dispersed metal oxide crystallites at a calcination temperature of 800 °C. The spheres are assumed to be a mixture of NiO, $Ca(OH)_2$, CaO and Ni-spinels. Furthermore, holes with different sizes were found on the surface of the catalysts, which could be attributed to the release of CO_2 during catalyst calcination [39]. In order to observe the catalyst structure, TEM images of selected catalysts with the ratio of Ca/Al of 1:1 and 3:1 are shown in Figure 3. For the Ni/$CaAlO_x$ (3:1) catalyst, it can be clearly seen that the surface was dominantly covered by rod-shaped $Ca(OH)_2$ with a size of around 15 nm, and NiO with a size of 10 nm which were sparsely embedded. This is in accordance with the crystal size calculated by XRD analysis (Figure 1), which shows a particle size of about 18.1 nm for $Ca(OH)_2$ and 9.3 nm for NiO, respectively. For the Ni/$CaAlO_x$ (1:1) catalyst, $Ca(OH)_2$ exhibited a spherical shape with a size of around 15 nm. NiO particles on the surface of the Ni/$CaAlO_x$ (1:1) catalyst have a similar size with that on the surface of the Ni/$CaAlO_x$ (3:1) catalyst, i.e. around 10 nm. The sizes of particles on the surface of the Ni/$CaAlO_x$ (1:1) catalyst observed by TEM are also consistent with the XRD analysis, i.e., 15.3 nm for $Ca(OH)_2$ and 9.0 nm for NiO, respectively. It is further suggested that

the increasing content of Ca in the catalysts increased the size of $Ca(OH)_2$, however it has little influence on the size of the active nickel-based phase in the $Ni/CaAlO_x$ catalysts.

The reducibility of $Ni/CaAlO_x$ catalysts with various Ca/Al molar ratios was investigated by H_2-TPR, and the reduction profiles are shown in Figure 4. All the fresh catalysts are characterized by three main reduction peaks: the first peak is centered at around 400 °C which might be assigned to the reduction of bulk NiO oxides [40]. The second reduction peak between 450 and 600 °C might be attributed to complex NiO species which have stronger interaction with the CaO modified Al_2O_3 support [41]. The third reduction peak around 800 °C could result from the reduction of $NiAl_2O_4$ spinel phases [42-44]. For the $Ni/CaAlO_x$ (1:3) catalyst with 19.7% CaO content, the intensities of the three peaks were similar, indicating that the three fractions of NiO species were evenly distributed. However, with the stepwise increase of CaO content to around 50%, the relative intensity of reduction peaks for bulk NiO showed an obvious increase. It indicates that the increase of Ca content in the $Ni/CaAlO_x$ catalysts contributes to the increase of the fraction of bulk NiO species. Hou et al. [40] reported that the presence of an excess amount of Ca ($Ca/Ni \geq 0.2$) in a $Ni\text{-}Ca/Al_2O_3$ catalyst prepared by impregnation method covered the surface of the Al_2O_3 support and hindered the interaction between Ni and support [41]. In this work, the increase of Ca content might occupy more surface area of the alumina support and reduce the interactions between Ni and the catalyst support; thus resulting in an increas in the fraction of bulk Ni-species with the increase of Ca content. In addition, the reducibility of a Ni-Al catalyst was reported to be increased by adding La metal [45].

3.2 Pyrolysis/steam reforming of sawdust over $Ni/CaAlO_x$ catalysts

Catalytic steam reforming of pyrolysis product gases derived from biomass sawdust pyrolysis was carried out at 800 °C to evaluate the performance of the developed catalysts with different Ca/Al molar ratios. The mass balance calculated for each experiment is shown in Table 2. Char residue was obtained in the pyrolysis stage. The yield of char residue in terms of the amount of biomass sample is around 38 wt.% for all the experiments, as the pyrolysis stage was not affected by the type of catalyst

downstream. Compared with pyrolysis-reforming of biomass without catalyst (using sand), it was found that with the addition of catalyst, the yields of total gas and hydrogen greatly increased, from around 30 to 50 wt.% and from 2 to >10 mmol g^{-1} biomass, respectively. It is difficult to determine a clear influence of Ca content on total gas yield from Table 2. Quincoces et al. [46] has also reported that there were no important influences of Ca addition on methane reforming; It was suggested that small modifications of crystal size were obtained for Ni-Al catalyst containing different amounts of Ca, which is consistent with our results in relation to the changes of crystal size as presented in Table 1. However, the highest gas yield (65.2 wt.%) was obtained using the Ni/$CaAlO_x$ (1:2) catalyst, which might be related to the catalyst with the highest BET surface area (Table 1), which promoted more contact between reactants and catalytic sites. In addition, the Ni/$CaAlO_x$ (1:1) catalyst showed a lower gas yield (55.87 wt.%) compared with the Ni/$CaAlO_x$ (1:2) and the Ni/$CaAlO_x$ (2:1) catalysts, which might also be due to the Ni/$CaAlO_x$ (1:1) catalyst which had a lower BET surface area (Table 1).

From Table 2, it seems that hydrogen production was increased slightly from 12.97 to 15.57 mmol g^{-1} biomass, when the catalyst was changed from the Ni/$CaAlO_x$ (1:3) to the Ni/$CaAlO_x$ (1:2); with the further increase of Ca content, the hydrogen production was reduced slightly to 14.32 mmol g^{-1} biomass using the Ni/$CaAlO_x$ (3:1) catalyst.

The performance of the catalyst during biomass pyrolysis-reforming was also compared using the product gas concentrations (N_2 carrier gas free), as shown in Figure 5. In the absence of catalyst, CO concentration was about 45 Vol.% and H_2 concentration was about 18 Vol.%. In the presence of Ni/$CaAlO_x$ catalyst, the concentration of H_2 increased markedly to about 45 Vol.%, and the concentration of CO reduced to about 30 Vol.% (except for the Ni/$CaAlO_x$ (3:1) catalyst). It is suggested that the water gas shift reaction (Reaction 1) was significantly enhanced by the introduction of the catalysts for the reforming of primary products from pyrolysis-reforming of wood sawdust [24, 47]. In addition, the concentrations of hydrocarbon gases (CH_4 and C_2-C_4) were largely reduced as shown in Figure 5 in the presence of catalyst, indicating steam reforming of

hydrocarbons (Reaction 2) was effectively promoted by adding the Ni-based catalyst prepared in this work.

$CO + H_2O \leftrightarrow CO_2 + H_2$ Reaction 1

$C_xH_y + 2xH_2O \rightarrow xCO_2 + (2x+y/2)H_2$ Reaction 2

$CO_2 + CH_4 \leftrightarrow 2CO + 2H_2$ Reaction 3

Hydrogen concentration was slightly changed when the catalysts with different Ca/Al molar ratios were used for thermo-chemical conversion of biomass. From Figure 5, CO concentration increased from about 30 to 45 Vol.%, and CO_2 concentration reduced from 20 to 12 Vol.%, when the molar ratio of Ca/Al was increased from 1:3 to 3:1 for the $Ni/CaAlO_x$ catalyst; this might be ascribed to the inhibition of the water gas shift reaction (WGSR) (Reaction 1). In addition, the reduction of CO_2 concentration with the increase of Ca content might be due to the promotion of CO_2 reforming reactions (e.g. Reaction 3). It is known that the acidic sites of nickel-based alumina catalysts resulted in coke deposition during reforming reactions [48]. The addition of Ca into a Ni-Al catalyst has been reported to significantly increase the basicity of the catalyst [49]. In this work, it is suggested that the increase of basic sites promoted the methane dry reforming reaction (Reaction 3) with the increase of Ca content in the $Ni/CaAlO_x$ catalyst; this is consistent with the other reports, where CO_2 conversion was enhanced during methane dry reforming by increasing the Ca content in a Ni-Ca-based catalyst [41].

Here, it is suggested that the addition of Ca promoted the metal dispersion and affected the equilibrium through adsorption on the enhanced basicity sites. NiO and $NiAl_2O_4$ (as identified in the XRD analysis of the fresh catalysts, Figure 1) have been reported to provide active Ni sites for methane dry reforming [50]. From the TPR analysis of the fresh catalysts, it seems that the fraction of NiO species was increased with the increase of Ca addition. Therefore, it is proposed that in this work, NiO species play key roles to provide active sites for methane dry reforming (Reaction 3) and possibly other hydrogen carbon reforming reactions for CO production. Ni has also been reported as active sites for the WGSR [51]; however, the increase of NiO fraction in the catalyst with the

increase of Ca addition did not enhance the WGSR. Here we suggested that the water gas shift reaction has been significantly affected by the basicity of the catalyst introduced by the addition of Ca.

From Figure 5, it is demonstrated that the concentration of syngas (H_2 and CO) was about 80 Vol.% using the Ni/$CaAlO_x$ (1:3) catalyst, and increased to about 90 Vol.% when the Ca/Al molar ratio was increased to 3:1 (the Ni/$CaAlO_x$(3:1) catalyst), while the concentration of H_2 was almost constant. In addition, with the addition of the catalyst, the H_2/CO molar ratio increased significantly to about 1.63 from 0.38. A range of H_2/CO molar ratio between 1.01 and 1.63 was obtained using different Ni/$CaAlO_x$ catalysts (Table 2). It is therefore suggested that using the Ni/$CaAlO_x$ catalyst prepared in this work the H_2/CO molar ratio in syngas can be manipulated, by controlling the content of Ca in the catalyst system; since it appears that the selectivity to CO or CO_2 was related to the Ca content in the Ni/$CaAlO_x$ catalyst.

3.3 Coke formation analysis using temperature programmed oxidation

Coke deposition is one of the most problematic factors causing catalyst deactivation during catalytic thermo-chemical conversion of biomass [52, 53]. The characteristics of coke formation on the reacted Ni/$CaAlO_x$ catalysts were investigated using temperature programmed oxidation (TPO). Figure 6 shows TGA results of TPO analysis for the reacted catalysts. It can be seen that two types of carbon were formed on the surface of the majority of the reacted catalysts corresponding to a two-stage weight loss. For all the catalysts except the Ni/$CaAlO_x$ (1:3), the weight loss which occurred at around 410 °C might be assigned to the oxidation of amorphous carbons. The weight loss at higher oxidation temperature (around 600 °C) might be assigned to filamentous carbon [54]. However the reacted Ni/$CaAlO_x$ (1:3) catalyst showed a three-stage weight loss in the TPO analysis, which occurred at around 270, 560 and 710 °C, respectively. The weight loss around 400 °C was normally deemed as heavy hydrocarbon depositions, and the one at 560 °C may be attributed to the oxidation of amorphous carbons [47, 55]; the weight loss at around 710 °C for the reacted Ni/$CaAlO_x$ (1:3) catalyst can be assigned to filamentous carbons for the reacted Ni/$CaAlO_x$ (1:3) catalyst [53, 56]. It is noted that

weight increase was observed at around 550 °C from Figure 6 in particular for the catalysts with high Ca content, demonstrating that oxidation of Ni might happened during the TPO analysis. It is known that Ni could be produced from the reduction of NiO during the pyrolysis-reforming reactions.

It was reported that high dispersion of nickel metal particles and the basicity of the support surface benefited the resistance to coke deposition, since water splitting into hydroxyl (OH^-) groups could be enhanced during reforming reactions due to the high nickel dispersion and support basicity, which thus promoted carbon elimination reaction with hydroxyl groups [14]. The use of Ni/Al_2O_3 catalysts in the thermo-chemical conversion process is known to have problems of coke deposition on the surface of the catalyst due to the presence of acid sites [48]. In this work, Ca was added to the catalyst system to improve the catalyst basicity in order to reduce coke formation during pyrolysis-reforming of biomass. It is reported that the increase of basicity of a catalyst by adding Ca could promote steam-coke reactions, which resulted in a decrease of coke deposition on the surface of the catalyst during the steam reforming of biomass [49]. The reacted $Ni/CaAlO_x$ (1:3) catalyst showed the highest coke formation (about 20 wt.%); this might be because the $Ni/CaAlO_x$ (1:3) catalyst has the lowest alkaline metal (Ca) addition which corresponded to the lowest catalyst basicity compared with the other $Ni/CaAlO_x$ catalysts. The amount of coke deposition on the surface of the reacted catalyst was estimated from the weight loss of reacted catalysts from the TPO analysis, with the assumption that the weight increase from Ni oxidation was insignificant.

For the other reacted $Ni/CaAlO_x$ catalysts, coke formation was less than 10 wt.% of the weight of the reacted catalyst. It seems that the coke deposition on the surface of the reacted catalyst was reduced when the Ca/Al molar ratio was increased from 1:3 to 3:1. However, as shown in Figure 6, amorphous carbon was largely formed on the reacted $Ni/CaAlO_x$ (3:1) catalyst (weight loss around 400 °C), indicating that there might be an optimal content of Ca addition to the catalyst in order to minimize coke formation. Amorphous carbons are known to easily deactivate catalyst by encapsulating catalytic active sites.

4. Conclusions

As an alkaline metal, Ca is attractive to promote catalytic activity in thermo-chemical conversion of biomass due to its low cost and high abundance in nature. In this study, a series of Ni/$CaAlO_x$ catalysts promoted by different contents of Ca were prepared by co-precipitation method, and were investigated for H_2-enriched syngas production from the pyrolysis-reforming of sawdust biomass. The following conclusions were proposed:

1) High dispersion of NiO particles was obtained within the Ni/$CaAlO_x$ catalysts. With the increase of Ca/Al molar ratio from 1:3 to 3:1, the particle size of NiO remained constant at around 10 nm, while the reducibility of the Ni/$CaAlO_x$ catalysts increased according to TPR analysis.

2) The catalytic performance in terms of total gas yield and hydrogen production was not closely related to the content of Ca in the catalyst. The total gas yield might depend on the surface area of the catalyst. The Ni/$CaAlO_x$ (1:3) catalyst showed the lowest gas production; this might be due to the severe catalyst deactivation which resulted from coke deposition which was supported from TPO analysis.

3) It was clearly demonstrated that the increase of Ca content resulted in the increase of CO selectivity and the decrease of CO_2 selectivity.

4) A total concentration of 90 Vol.% syngas (H_2 + CO) could be obtained using the Ni/$CaAlO_x$ (3:1) catalyst. In addition, the H_2/CO ratio could be controlled between 1.01 and 1.63 by varying Ca content while H_2 concentration in the syngas remained almost constant. This is particularly important in relation to the manipulation of syngas composition for downstream applications

Acknowledgements

This work was supported by the International Exchange Scheme from the Royal Society (IE110273), UK, and the Faculty of Engineering & IT Cluster Scheme from the University of Sydney.

References

[1] A. Neumann, C. von Hirschhausen, Natural Gas: An Overview of a Lower-Carbon Transformation Fuel, Review of Environmental Economics and Policy, 9 (2015) 64-84.
[2] Y. Wu, P. Zhao, H. Zhang, Y. Wang, G. Mao, Assessment for Fuel Consumption and Exhaust Emissions of China's Vehicles: Future Trends and Policy Implications, Scientific World Journal, (2012).
[3] P. Guo, P.J. van Eyk, W.L. Saw, P.J. Ashman, G.J. Nathan, E.B. Stechel, Performance Assessment of Fischer-Tropsch Liquid Fuels Production by Solar Hybridized Dual Fluidized Bed Gasification of Lignite, Energy & Fuels, 29 (2015) 2738-2751.
[4] M. Al-Dossary, J.L.G. Fierro, J.J. Spivey, Cu-Promoted Fe2O3/MgO-Based Fischer-Tropsch Catalysts of Biomass-Derived Syngas, Industrial & Engineering Chemistry Research, 54 (2015) 911-921.
[5] A. Corsaro, T. Wiltowski, D. Juchelova, The Conversion of Syngas to Liquid Fuels in a Dual-Bed Single Reactor Process, Petroleum Science and Technology, 32 (2014) 2722-2729.
[6] K. Liu, C. Song, V. Subramani, Hydrogen and syngas production and purification technologies, John Wiley & Sons, New Jersey, 2010.
[7] A.F. Kirkels, G.P.J. Verbong, Biomass gasification: Still promising? A 30-year global overview, Renewable and Sustainable Energy Reviews, 15 (2011) 471-481.
[8] P. Parthasarathy, K.S. Narayanan, Hydrogen production from steam gasification of biomass: Influence of process parameters on hydrogen yield – A review, Renewable Energy, 66 (2014) 570-579.
[9] A.C. Caputo, M. Palumbo, P.M. Pelagagge, F. Scacchia, Economics of biomass energy utilization in combustion and gasification plants: effects of logistic variables, Biomass and Bioenergy, 28 (2005) 35-51.
[10] G.W. Huber, S. Iborra, A. Corma, Synthesis of transportation fuels from biomass: Chemistry, catalysts, and engineering, Chemical Reviews, 106 (2006) 4044-4098.
[11] A. Demirbas, Hydrogen production from biomass by the gasification process, Energy Sources, 24 (2002) 59-68.
[12] Y. Kalinci, A. Hepbasli, I. Dincer, Biomass-based hydrogen production: A review and analysis, International Journal of Hydrogen Energy, 34 (2009) 8799-8817.
[13] Y. Shen, K. Yoshikawa, Recent progresses in catalytic tar elimination during biomass gasification or pyrolysis—A review, Renewable and Sustainable Energy Reviews, 21 (2013) 371-392.
[14] M. Ni, D.Y.C. Leung, M.K.H. Leung, A review on reforming bio-ethanol for hydrogen production, International Journal of Hydrogen Energy, 32 (2007) 3238-3247.
[15] A. Erkiaga, G. Lopez, M. Amutio, J. Bilbao, M. Olazar, Steam gasification of biomass in a conical spouted bed reactor with olivine and γ-alumina as primary catalysts, Fuel Processing Technology, 116 (2013) 292-299.
[16] B.S. Huang, H.Y. Chen, K.H. Chuang, R.X. Yang, M.Y. Wey, Hydrogen production by biomass gasification in a fluidized-bed reactor promoted by an Fe/CaO catalyst, International Journal of Hydrogen Energy, 37 (2012) 6511-6518.
[17] S. Cheah, K.R. Gaston, Y.O. Parent, M.W. Jarvis, T.B. Vinzant, K.M. Smith, N.E. Thornburg, M.R. Nimlos, K.A. Magrini-Bair, Nickel cerium olivine catalyst for catalytic gasification of biomass, Applied Catalysis B-Environmental, 134 (2013) 34-45.

[18] K. Tomishige, M. Asadullah, K. Kunimori, Syngas production by biomass gasification using Rh/CeO2/SiO2 catalysts and fluidized bed reactor, Catalysis Today, 89 (2004) 389-403.
[19] J. Wambach, M. Schubert, M. Doebeli, F. Vogel, Characterization of a Spent Ru/C Catalyst after Gasification of Biomass in Supercritical Water, Chimia, 66 (2012) 706-711.
[20] M. Marono, J.M. Sanchez, E. Ruiz, A. Cabanillas, Study of the Suitability of a Pt-Based Catalyst for the Upgrading of a Biomass Gasification Syngas Stream via the WGS Reaction, Catalysis Letters, 126 (2008) 396-406.
[21] K. Nakamura, T. Miyazawa, T. Sakurai, T. Miyao, S. Naito, N. Begum, K. Kunimori, K. Tomishige, Promoting effect of MgO addition to Pt/Ni/CeO2/Al2O3 in the steam gasification of biomass, Applied Catalysis B-Environmental, 86 (2009) 36-44.
[22] L. Chen, C.K.S. Choong, Z. Zhong, L. Huang, Z. Wang, J. Lin, Support and alloy effects on activity and product selectivity for ethanol steam reforming over supported nickel cobalt catalysts, International Journal of Hydrogen Energy, 37 (2012) 16321-16332.
[23] C. Wu, L. Dong, J. Onwudili, P.T. Williams, J. Huang, Effect of Ni Particle Location within the Mesoporous MCM-41 Support for Hydrogen Production from the Catalytic Gasification of Biomass, Acs Sustainable Chemistry & Engineering, 1 (2013) 1083-1091.
[24] C. Wu, L. Wang, P.T. Williams, J. Shi, J. Huang, Hydrogen production from biomass gasification with Ni/MCM-41 catalysts: Influence of Ni content, Applied Catalysis B-Environmental, 108 (2011) 6-13.
[25] P.R. Buchireddy, R.M. Bricka, J. Rodriguez, W. Holmes, Biomass Gasification: Catalytic Removal of Tars over Zeolites and Nickel Supported Zeolites, Energy & Fuels, 24 (2010) 2707-2715.
[26] J. Tao, L. Zhao, C. Dong, Q. Lu, X. Du, E. Dahlquist, Catalytic Steam Reforming of Toluene as a Model Compound of Biomass Gasification Tar Using Ni-CeO2/SBA-15 Catalysts, Energies, 6 (2013) 3284-3296.
[27] Y. Zhang, R. Xiao, X. Gu, H. Zhang, D. Shen, G. He, Catalytic Pyrolysis of Biomass with Fe/La/SBA-15 Catalyst using TGA-FTIR Analysis, Bioresources, 9 (2014) 5234-5245.
[28] J. Zhu, X. Peng, L. Yao, D. Tong, C. Hu, CO2 reforming of methane over Mg-promoted Ni/SiO2 catalysts: the influence of Mg precursors and impregnation sequences, Catalysis Science & Technology, 2 (2012) 529-537.
[29] D.K. Kim, K. Stöwe, F. Müller, W.F. Maier, Mechanistic study of the unusual catalytic properties of a new NiCe mixed oxide for the CO2 reforming of methane, Journal of Catalysis, 247 (2007) 101-111.
[30] D. Liu, X.Y. Quek, W.N.E. Cheo, R. Lau, A. Borgna, Y. Yang, MCM-41 supported nickel-based bimetallic catalysts with superior stability during carbon dioxide reforming of methane: Effect of strong metal–support interaction, Journal of Catalysis, 266 (2009) 380-390.
[31] A. Arslan, S. Gunduz, T. Dogu, Steam reforming of ethanol with zirconia incorporated mesoporous silicate supported catalysts, International Journal of Hydrogen Energy, 39 (2014) 18264-18272.
[32] C. Wu, P.T. Williams, A novel Ni–Mg–Al–CaO catalyst with the dual functions of catalysis and CO2 sorption for H2 production from the pyrolysis–gasification of polypropylene, Fuel, 89 (2010) 1435-1441.
[33] N. Gao, S. Liu, Y. Han, C. Xing, A. Li, Steam reforming of biomass tar for hydrogen production over NiO/ceramic foam catalyst, International Journal of Hydrogen Energy, 40 (2015) 7983-7990.
[34] S. Limmanee, T. Naree, K. Bunyakiat, C. Ngamcharussrivichai, Mixed oxides of Ca, Mg and Zn as heterogeneous base catalysts for the synthesis of palm kernel oil methyl esters, Chemical Engineering Journal, 225 (2013) 616-624.

[35] Y. Kobayashi, J. Horiguchi, S. Kobayashi, Y. Yamazaki, K. Omata, D. Nagao, M. Konno, M. Yamada, Effect of NiO content in mesoporous NiO–Al2O3 catalysts for high pressure partial oxidation of methane to syngas, Applied Catalysis A: General, 395 (2011) 129-137.
[36] D. Dissanayake, M.P. Rosynek, K.C.C. Kharas, J.H. Lunsford, Partial oxidation of methane to carbon monoxide and hydrogen over a Ni/Al2O3 catalyst, Journal of Catalysis, 132 (1991) 117-127.
[37] G.W. Wu, S.R. Li, C.X. Zhang, T. Wang, J.L. Gong, Glycerol steam reforming over perovskite-derived nickel-based catalysts, Applied Catalysis B-Environmental, 144 (2014) 277-285.
[38] K.F.M. Elias, A.F. Lucrédio, E.M. Assaf, Effect of CaO addition on acid properties of Ni–Ca/Al2O3 catalysts applied to ethanol steam reforming, International Journal of Hydrogen Energy, 38 (2013) 4407-4417.
[39] N. Sahli, C. Petit, A.C. Roger, A. Kiennemann, S. Libs, M.M. Bettahar, Ni catalysts from NiAl2O4 spinel for CO2 reforming of methane, Catalysis Today, 113 (2006) 187-193.
[40] C. Wu, L. Wang, P.T. Williams, J. Shi, J. Huang, Hydrogen production from biomass gasification with Ni/MCM-41 catalysts: Influence of Ni content, Applied Catalysis B: Environmental, 108–109 (2011) 6-13.
[41] Z. Hou, O. Yokota, T. Tanaka, T. Yashima, Characterization of Ca-promoted Ni/α-Al2O3 catalyst for CH4 reforming with CO2, Applied Catalysis A: General, 253 (2003) 381-387.
[42] E. Salehi, F.S. Azad, T. Harding, J. Abedi, Production of hydrogen by steam reforming of bio-oil over Ni/Al2O3 catalysts: Effect of addition of promoter and preparation procedure, Fuel Processing Technology, 92 (2011) 2203-2210.
[43] F. Seyedeyn Azad, J. Abedi, E. Salehi, T. Harding, Production of hydrogen via steam reforming of bio-oil over Ni-based catalysts: Effect of support, Chemical Engineering Journal, 180 (2012) 145-150.
[44] H.-S. Roh, K.Y. Koo, U.H. Jung, W.L. Yoon, Hydrogen production from natural gas steam reforming over Ni catalysts supported on metal substrates, Current Applied Physics, 10 (2010) S37-S39.
[45] Martı, amp, x, R. nez, E. Romero, Garcı, amp, x, L. a, R. Bilbao, The effect of lanthanum on Ni–Al catalyst for catalytic steam gasification of pine sawdust, Fuel Processing Technology, 85 (2004) 201-214.
[46] C.E. Quincoces, S. Dicundo, A.M. Alvarez, M.G. González, Effect of addition of CaO on Ni/Al2O3 catalysts over CO2 reforming of methane, Materials Letters, 50 (2001) 21-27.
[47] C. Wu, Z. Wang, J. Huang, P.T. Williams, Pyrolysis/gasification of cellulose, hemicellulose and lignin for hydrogen production in the presence of various nickel-based catalysts, Fuel, 106 (2013) 697-706.
[48] K. Urasaki, K. Tokunaga, Y. Sekine, M. Matsukata, E. Kikuchi, Production of hydrogen by steam reforming of ethanol over cobalt and nickel catalysts supported on perovskite-type oxides, Catalysis Communications, 9 (2008) 600-604.
[49] J. Ashok, Y. Kathiraser, M.L. Ang, S. Kawi, Bi-functional hydrotalcite-derived NiO–CaO–Al2O3 catalysts for steam reforming of biomass and/or tar model compound at low steam-to-carbon conditions, Applied Catalysis B: Environmental, 172–173 (2015) 116-128.
[50] S. Wang, A Comprehensive Study on Carbon Dioxide Reforming of Methane over Ni/γ-Al2O3 Catalysts, Industrial & Engineering Chemistry Research, 38 (1999) 2615-2625.
[51] J. Carrasco, D. López-Durán, Z. Liu, T. Duchoň, J. Evans, S.D. Senanayake, E.J. Crumlin, V. Matolín, J.A. Rodríguez, M.V. Ganduglia-Pirovano, In Situ and Theoretical Studies for the Dissociation of Water on an Active Ni/CeO2 Catalyst: Importance of Strong Metal–Support

Interactions for the Cleavage of O–H Bonds, Angewandte Chemie International Edition, 54 (2015) 3917-3921.
[52] T. Horiuchi, K. Sakuma, T. Fukui, Y. Kubo, T. Osaki, T. Mori, Suppression of carbon deposition in the CO 2-reforming of CH 4 by adding basic metal oxides to a Ni/Al 2O 3 catalyst, Applied Catalysis A: General, 144 (1996) 111-120.
[53] S. Helveg, J. Sehested, J.R. Rostrup-Nielsen, Whisker carbon in perspective, Catalysis Today, 178 (2011) 42-46.
[54] C. Wu, P.T. Williams, Investigation of coke formation on Ni-Mg-Al catalyst for hydrogen production from the catalytic steam pyrolysis-gasification of polypropylene, Applied Catalysis B: Environmental, 96 (2010) 198-207.
[55] B.S. Liu, C.T. Au, Carbon deposition and catalyst stability over La2NiO4/γ-Al2O3 during CO2 reforming of methane to syngas, Applied Catalysis A: General, 244 (2003) 181-195.
[56] C.F. Wu, P.T. Williams, Hydrogen production from steam reforming of ethanol with nano-Ni/SiO2 catalysts prepared at different Ni to citric acid ratios using a sol-gel method, Applied Catalysis B-Environmental, 102 (2011) 251-259.

Table 1 Composition, particle size and surface areas of the $Ni/CaAlO_x$ catalysts

Catalyst	**Molar Ratio (Ca/Al)**	**Metal molar composition (wt.%)[a]**			**Particle size (nm)[b]**				**BET surface area (m^2g^{-1})**
		NiO	CaO	Al_2O_3	$Ca(OH)_2$	CaO	$NiAl_2O_4$	NiO	
$Ni/CaAlO_x$	1:3	26.4	19.7	53.9	14.0	15.6	19.5	9.7	64.6
	1:2	26.3	26.1	47.6	15.0	17.1	11.9	11.3	83.0
	1:1	25.9	38.8	35.3	15.3	16.2	13.2	9.0	46.8
	2:1	25.6	51.1	23.2	16.6	13.3	-	10.8	61.0
	3:1	25.5	57.1	17.3	18.1	19.4	-	9.3	46.3

[a]-Molar ratio was obtained from calculation of catalyst preparation; [b]- Particle size was calculated from XRD analysis using the Scherrer equation.

Table 2 Mass balance for pyrolysis catalytic steam reforming of biomass using $Ni/CaAlO_x$ catalyst

Catalyst Bed	**Sand**	**Catalyst with different Ca/Al ratios**				
		1:3	1:2	1:1	2:1	3:1
Gas/biomass (wt.%)	32.99	55.42	65.2	55.87	63.45	57.57
Residue char/biomass (wt.%)	38.75	36.25	37.5	37.5	37.5	37.5
Mass balance (wt.%)	103.25	104.29	97.03	95.69	98.67	95.95
H_2 Yield (mmol H_2 g^{-1} biomass)	2.36	12.97	15.57	15.3	15.37	14.32
H_2/CO molar ratio	0.38	1.51	1.08	1.63	1.25	1.01

Figure Captions

Figure 1 XRD patterns of Ni/$CaAlO_x$ catalysts: (a) Ni/$CaAlO_x$ (1:3); (b) Ni/$CaAlO_x$ (1:2); (c) Ni/$CaAlO_x$ (1:1); (d) Ni/$CaAlO_x$ (2:1); (e) Ni/$CaAlO_x$ (3:1).

Figure 2 SEM imagines of the fresh Ni/$CaAlO_x$ catalysts. (a) Ni/$CaAlO_x$ (1:3); (b) Ni/$CaAlO_x$ (1:2); (c) Ni/$CaAlO_x$ (1:1); (d) Ni/$CaAlO_x$ (2:1); (e) Ni/$CaAlO_x$ (3:1).

Figure 3 TEM images of the fressh Ni/$CaAlO_x$ catalysts. (a) Ni/$CaAlO_x$ (3:1); (b) Ni/$CaAlO_x$ (1:1)

Figure 4 TPR results of the Ni/$CaAlO_x$ catalysts: (a) Ni/$CaAlO_x$ (1:3); (b) Ni/$CaAlO_x$ (1:2); (c) Ni/$CaAlO_x$ (1:1); (d) Ni/$CaAlO_x$ (2:1); (e) Ni/$CaAlO_x$ (3:1).

Figure 5 Gas compositions and fractions from biomass gasification on the sand and Ni/$CaAlO_x$ catalysts. (a) sand; (b) Ni/$CaAlO_x$ (1:3); (c) Ni/$CaAlO_x$ (1:2); (d) Ni/$CaAlO_x$ (1:1); (e) Ni/$CaAlO_x$ (2:1); (f) Ni/$CaAlO_x$ (3:1).

Figure 6 TPO analyses of reacted Ni/$CaAlO_x$ catalysts: (a) Ni/$CaAlO_x$ (1:3); (b) Ni/$CaAlO_x$ (1:2); (c) Ni/$CaAlO_x$ (1:1); (d) Ni/$CaAlO_x$ (2:1); (e) Ni/$CaAlO_x$ (3:1).

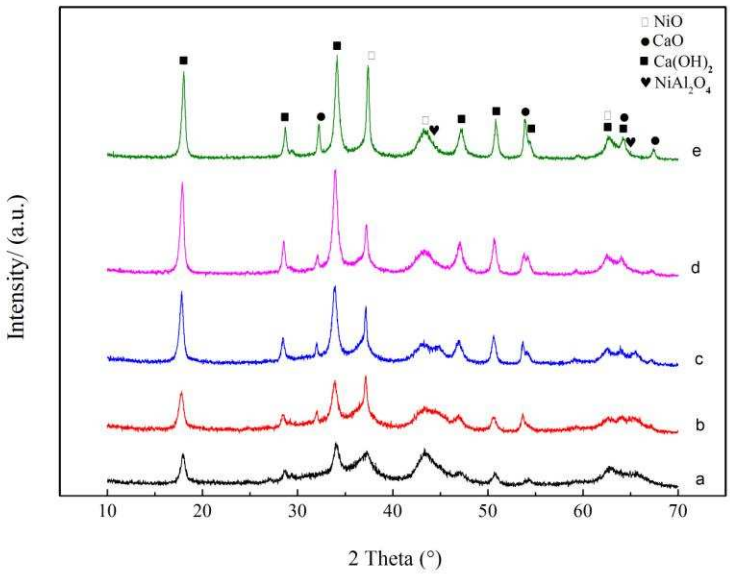

Figure 1 XRD patterns of $Ni/CaAlO_x$ catalysts: (a) $Ni/CaAlO_x$ (1:3); (b) $Ni/CaAlO_x$ (1:2); (c) $Ni/CaAlO_x$ (1:1); (d) $Ni/CaAlO_x$ (2:1); (e) $Ni/CaAlO_x$ (3:1).

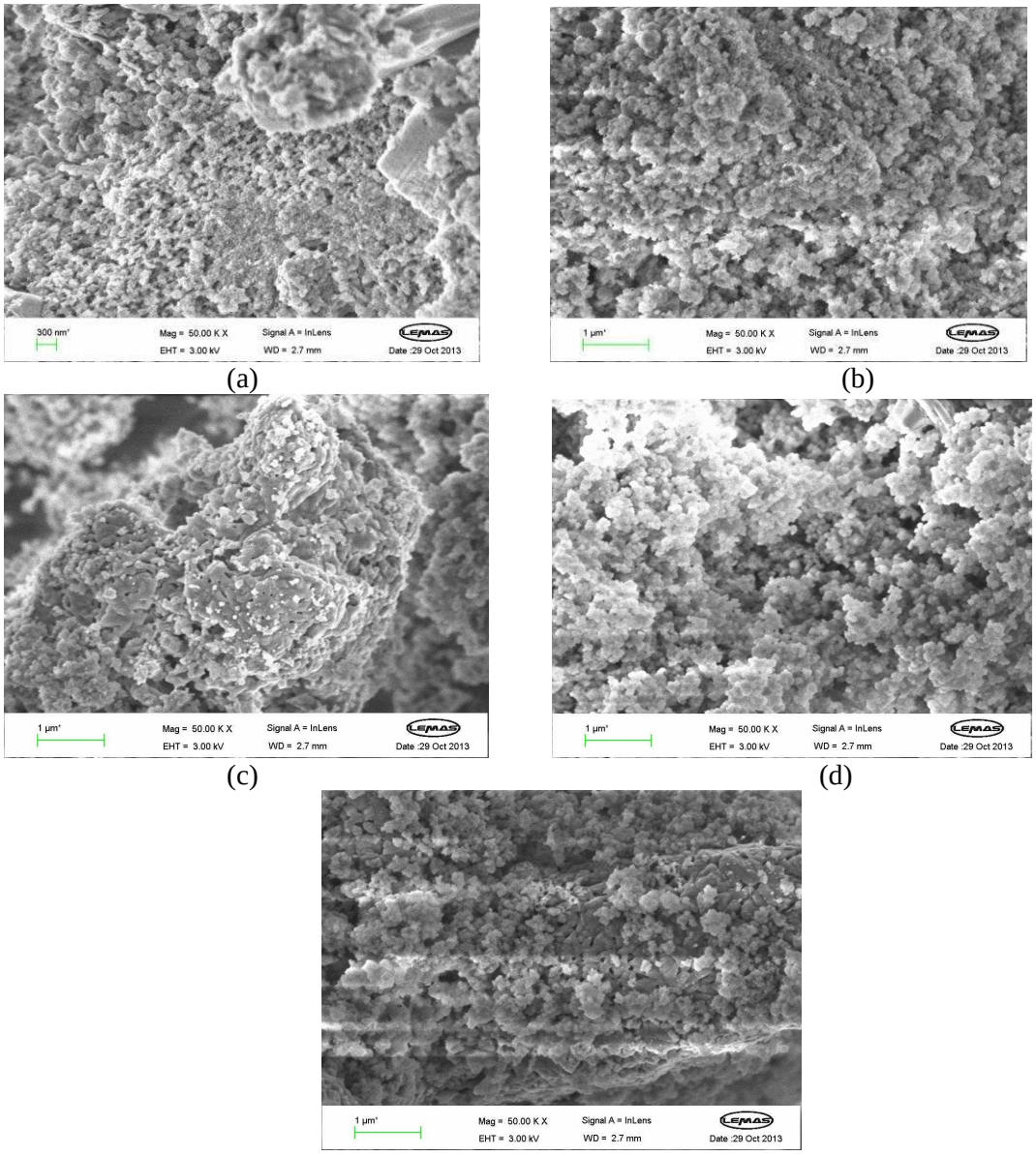

Figure 2 SEM imagines of the fresh $Ni/CaAlO_x$ catalysts. (a) $Ni/CaAlO_x$ (1:3); (b) $Ni/CaAlO_x$ (1:2); (c) $Ni/CaAlO_x$ (1:1); (d) $Ni/CaAlO_x$ (2:1); (e) $Ni/CaAlO_x$ (3:1).

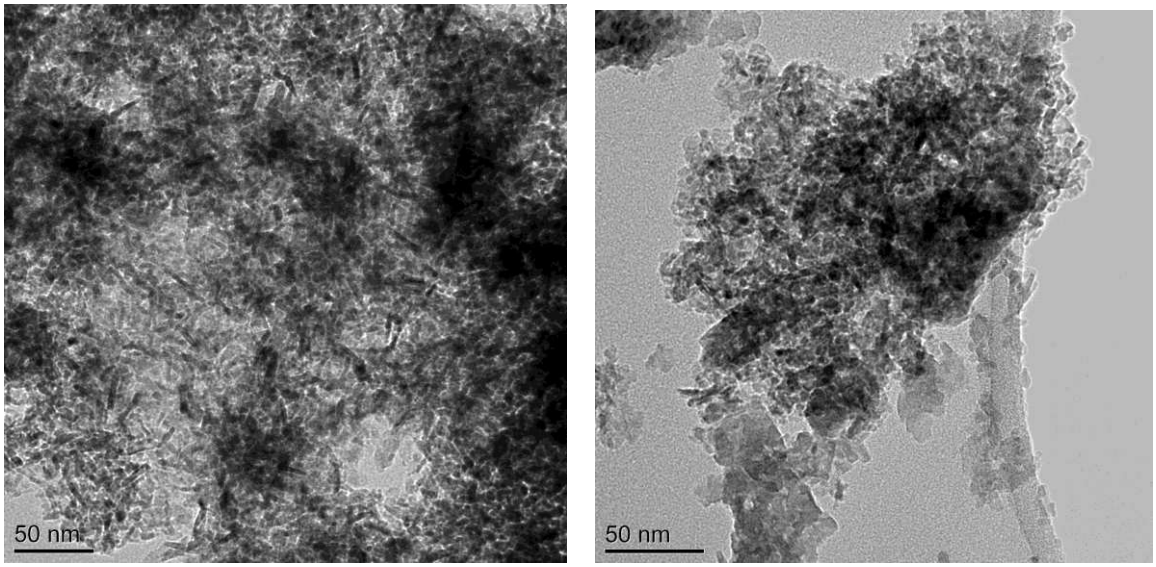

(a) (b)

Figure 3 TEM images of the fresh $Ni/CaAlO_x$ catalysts. (a) $Ni/CaAlO_x$ (3:1); (b) $Ni/CaAlO_x$ (1:1)

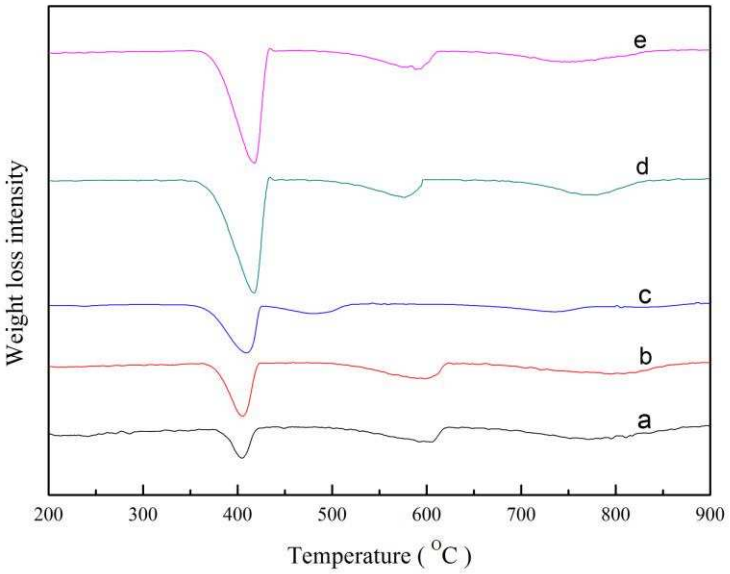

Figure 4 TPR results of the $Ni/CaAlO_x$ catalysts: (a) $Ni/CaAlO_x$ (1:3); (b) $Ni/CaAlO_x$ (1:2); (c) $Ni/CaAlO_x$ (1:1); (d) $Ni/CaAlO_x$ (2:1); (e) $Ni/CaAlO_x$ (3:1).

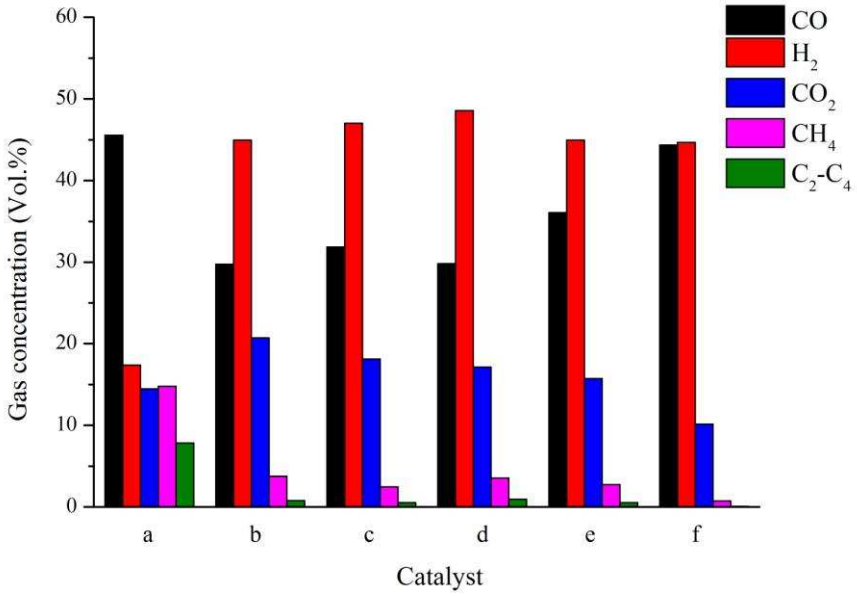

Figure 5 Gas compositions and fractions from biomass gasification on the sand and $Ni/CaAlO_x$ catalysts. (a) sand; (b) $Ni/CaAlO_x$ (1:3); (c) $Ni/CaAlO_x$ (1:2); (d) $Ni/CaAlO_x$ (1:1); (e) $Ni/CaAlO_x$ (2:1); (f) $Ni/CaAlO_x$ (3:1).

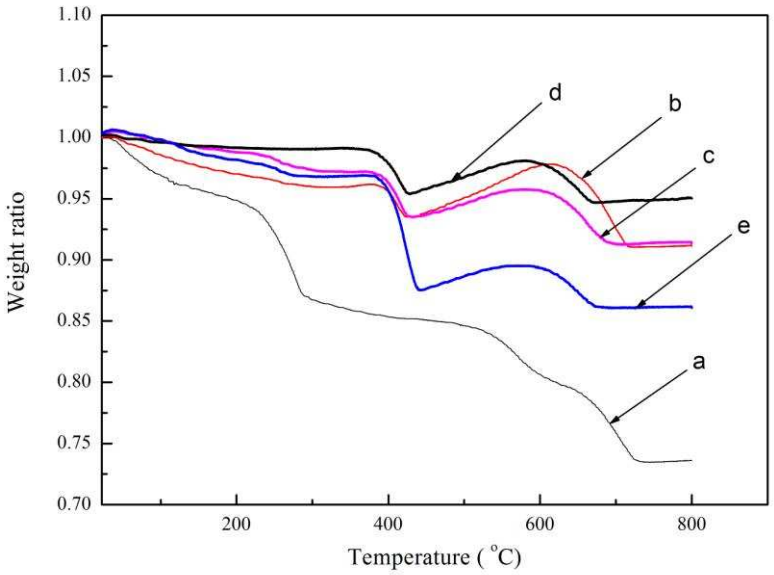

Figure 6 TPO analyses of reacted $Ni/CaAlO_x$ catalysts: (a) $Ni/CaAlO_x$ (1:3); (b) $Ni/CaAlO_x$ (1:2); (c) $Ni/CaAlO_x$ (1:1); (d) $Ni/CaAlO_x$ (2:1); (e) $Ni/CaAlO_x$ (3:1).